View metadata, citation and similar papers at core.ac.uk

brought to you by CORE

provided by Repositório da Universidade Nova de Lisboa

catalysts

MDPI

Article

Porphyrin–Nanodiamond Hybrid Materials—Active, Stable and Reusable Cyclohexene Oxidation Catalysts

Lucas D. Dias [1,2,*], Fábio M. S. Rodrigues [1], Mário J. F. Calvete [1], Sónia A. C. Carabineiro [3,4,*], Marisa D. Scherer [5], Anderson R. L. Caires [5,6], Josephus G. Buijnsters [7], José L. Figueiredo [3], Vanderlei S. Bagnato [2,8] and Mariette M. Pereira [1,*]

1 Departamento de Química, CQC, Universidade de Coimbra, Rua Larga, 3004-535 Coimbra, Portugal; fmsrodrigues.qui@gmail.com (F.M.S.R.); mcalvete@qui.uc.pt (M.J.F.C.)
2 São Carlos Institute of Physics, University of São Paulo, São Carlos 13566-590, Brazil; vander@ifsc.usp.br
3 Laboratory of Catalysis and Materials, Associate Laboratory LSRE-LCM, Faculty of Engineering, University of Porto, Rua Dr. Roberto Frias s/n, 4200-465 Porto, Portugal; jlfig@fe.up.pt
4 LAQV-REQUIMTE, Department of Chemistry, NOVA School of Science and Technology, Universidade NOVA de Lisboa, Quinta da Torre, 2829-516 Caparica, Portugal
5 Grupo de Óptica e Fotônica, Universidade Federal de Mato Grosso do Sul, CP 549, Campo Grande 79070-900, Brazil; marisa_bio_scherer@hotmail.com (M.D.S.); anderson.caires@ufms.br (A.R.L.C.)
6 School of Life Sciences, University of Essex, Colchester CO4 3SQ, UK
7 Department of Precision and Microsystems Engineering, Micro and Nano Engineering, Delft University of Technology, 2628 CD Delft, The Netherlands; J.G.Buijnsters@tudelft.nl
8 Hagler Fellow, Department of Biomedical Engineering, Texas A&M University–College Station Texas, 400 Bizzell St, College Station, TX 77843, USA
* Correspondence: lucas.dias1@usp.br (L.D.D.); sonia.carabineiro@fct.unl.pt (S.A.C.C.); mmpereira@qui.uc.pt (M.M.P.); Tel.: +55-16-3373-9810 (L.D.D.); +351-21294857 (S.A.C.C.); +351-239-852080 (M.M.P.)

Received: 9 October 2020; Accepted: 27 November 2020; Published: 1 December 2020

Abstract: The quest for active, yet "green" non-toxic catalysts is a continuous challenge. In this work, covalently linked hybrid porphyrin–nanodiamonds were prepared via *ipso* nitro substitution reaction and characterized by X-ray photoelectron spectroscopy (XPS), fluorescence spectroscopy, infrared spectroscopy (IR) and thermogravimetry-differential scanning calorimetry (TG-DSC). The amine-functionalized nanodiamonds (ND@NH_2) and 2-nitro-5,10,15,20-tetra(4-trifluoromethylphenyl)porphyrin covalently linked to nanodiamonds (ND@βNH-TPP*p*CF_3) were tested using *Allium cepa* as a plant model, and showed neither phytotoxicity nor cytotoxicity. The hybrid nanodiamond–copper(II)–porphyrin material ND@βNH-TPP*p*CF_3-Cu(II) was also evaluated as a reusable catalyst in cyclohexene allylic oxidation, and displayed a remarkable turnover number (TON) value of ≈265,000, using O_2 as green oxidant, in the total absence of sacrificial additives, which is the highest activity ever reported for said allylic oxidation. Additionally, ND@βNH-TPP*p*CF_3-Cu(II) could be easily separated from the reaction mixture by centrifugation, and reused in three consecutive catalytic cycles without major loss of activity.

Keywords: nanodiamonds; copper (II) porphyrin; allylic oxidation

1. Introduction

The recent advances of nanotechnology are remarkable. Nanostructured materials are part of our lives and a driving force towards the global economy of modern society. Among the many examples

available, the nanoallotropes of carbon are a unique family, among which nanodiamonds (NDs) are included. These carbon nanomaterials were first prepared by detonation in the USSR in the 1960s [1], and have been an exquisite research subject for many groups ever since, attracting tremendous interest, given their specific optical and physical/chemical properties [2].

Along with good biomedical compatibility, high adsorption capacity and large surface area, one of the most important characteristics of NDs is the presence of sp^2 carbon atoms in their structure [3]. As a result of the production method (detonation), the sp^3 diamond core is always covered with a few layers of sp^2 carbon. This allows surface functionalization, allowing the formation of electrostatic [4–6] or covalent linkages, and facilitating the preparation of hybrid organic–nanodiamond materials [7,8]. This has greatly contributed to a widespread application of these organic–nanodiamond carbon materials [9–14], in biomedicine [15–18], nonlinear optical materials [19,20], energy devices [21,22] and tribology [23,24].

Among the several hybrids consisting of ND and organic materials, we highlight those bearing tetrapyrrolic macrocycles, such as porphyrins [25] and phthalocyanines [1–6]. These are compounds with unique properties, used in a large range of biomedical applications [26–29] and as highly efficient catalysts in a variety of reactions [30,31].

It is expected that the synergism between ND properties, namely, biocompatibility, unique optical features, good thermal conductivity, electrical resistivity, resistance to harsh environments, and chemical stability [2] and the properties of tetrapyrrolic macrocycles, may pave the way for multiple additional applications. In this regard, only a few reports have been published on the preparation of hybrid ND–porphyrin materials, through the formation of either electrostatic bonds [32] or amide bonds between carboxy-phenyl-porphyrin and amino-functionalized NDs [19,25] (Scheme 1).

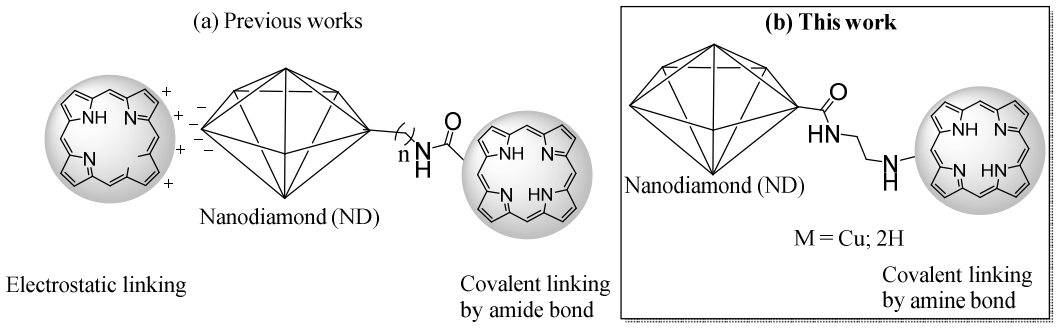

Scheme 1. Strategies for preparation of porphyrin–ND hybrid materials: (**a**) Previous works [19,25,32]; (**b**) this work.

The relatively low stability of these linkages against pH alterations or hydrolysis prompted us to devise and further establish an innovative synthetic strategy to immobilize porphyrins onto aminated functionalized NDs, via *ipso*-nitro substitution reaction with β-nitro substituted porphyrins, allowing the formation of much more stable covalent amine linkages. These new materials were fully characterized by X-ray photoelectron spectroscopy (XPS), thermogravimetry-differential scanning calorimetry (TG-DSC), fluorescence spectroscopy, infrared spectroscopy (IR) and ultraviolet–visible spectroscopy (UV–Vis).

Furthermore, the new hybrid nanodiamond–copper(II)–porphyrin ND@βNH-TPP*p*CF_3-Cu(II) was used as a catalyst in the oxidation of cyclohexene, using O_2 as a green oxidant. The oxidation of cyclohexene is of great interest, as its products (key C6 chemicals) are largely used as intermediates in the pharmaceutical/chemical industries [33,34]. A wide variety of catalysts have been used for the oxidation of cyclohexene with O_2 as an oxidant, such as ionic liquids; metal complexes, including metalloporphyrins; noble metals; and metal complexes immobilized on solid supports (carbon nanotubes, magnetic nanoparticles, titanium dioxide), as reported in a recent review [35]. However, controllable oxidation reactions that can selectively yield 7-oxabicyclo [4.1.0] heptane, trans/cis-cyclohexane-1,2-diol,

cyclohex-2-en-1-ol, cyclohex-2-en-1-one and adipic acid, using O_2 as a green oxidant, in solvent-free conditions, and using a stable, reusable and non-toxic catalyst, are still a challenge.

In this regard, the development of more sustainable practices is imperative in chemistry. Catalytic systems with negligible effects on the surrounding environments are desirable, but attention is usually paid to the substrate–product binomial, leaving catalysts out of the ecological concerns. Despite the increasing applications of NDs in bio- and nanomedicine [11,36], studies regarding their ecotoxic and genotoxic effects are still limited [37–41]. Herein, we also present a study on the cytotoxic and genotoxic evaluation of amine-functionalized nanodiamonds (ND@NH_2) and 2-nitro-5,10,15,20-tetra(4-trifluoromethylphenyl)porphyrin covalently linked to nanodiamonds (ND@βNH-TPP*p*CF_3) using *Allium cepa* as a plant model, as we aimed to obtain non-fitotoxic "green" catalysts—that is, materials that will not harm the environment (even if, accidentally, not properly discarded). *A. cepa* is largely used in genotoxicity studies, since it has a reduced number of large chromosomes, where changes are easy to detect. Additionally, the effects observed in its cells show good correlations with those of mammal (including human) cells [42].

2. Results

2.1. Synthesis and Characterization of Porphyrin-Functionalized Nanodiamonds (ND@βNH-TPPpCF$_3$-Cu(II) and ND@βNH-TPPpCF$_3$)

The porphyrins **1** and **2** were prepared by a previously reported methodology [30], using the nitrobenzene method [43], followed by nitration reaction with copper(II) nitrate to obtain porphyrin **1** and further demetallation with TFA to yield porphyrin **2**. The hybrid nanomaterials ND@βNH-TPP*p*CF_3-Cu(II) and ND@βNH-TPP*p*CF_3 involved the covalent grafting of the previously prepared nitro-porphyrins **1** and **2** onto (commercial) amine-functionalized nanodiamonds (ND@NH_2), via a typical *ipso*-nitro-aromatic nucleophilic substitution, where the presence of the strong electron withdrawing nitro group allows a direct nucleophilic substitution by amines [44–47], using Cs_2CO_3 as base and DME as solvent (Scheme 2). Further details can be found in the experimental section.

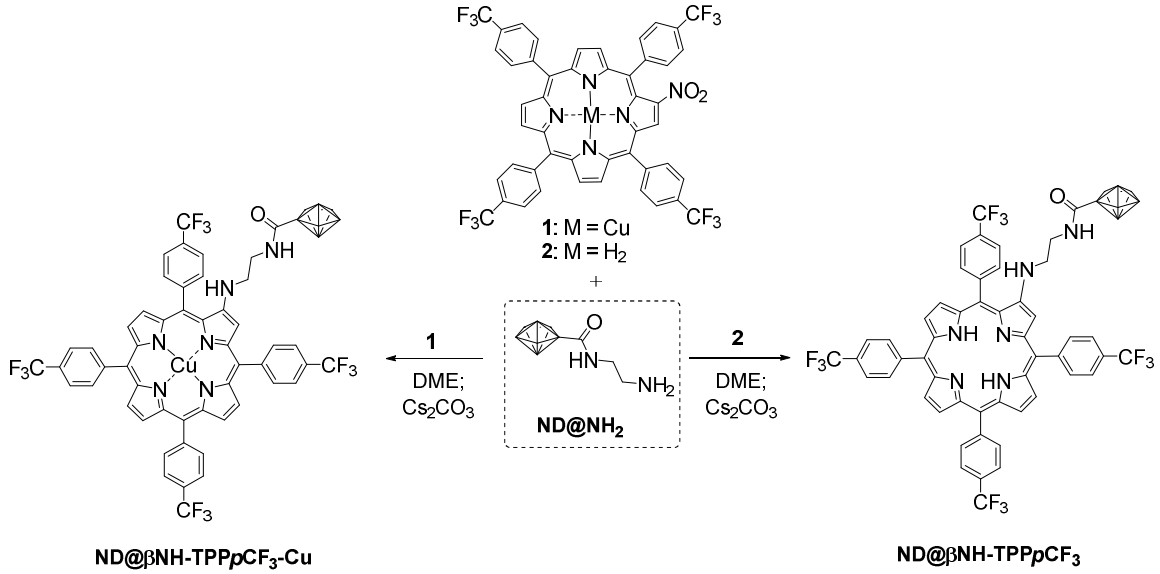

Scheme 2. Preparation of porphyrin-functionalized nanodiamonds (ND@βNH-TPP*p*CF_3-Cu(II) and ND@βNH-TPP*p*CF_3).

The hybrid materials were fully characterized by XPS, UV–Vis, fluorescence spectroscopy, Fourier transform infrared spectroscopy (FT-IR) and thermogravimetry-differential scanning calorimetry (TG-DSC). The quantification of immobilized-nitro porphyrin (**1** and **2**) on the functionalized NDs (primary average particle size of 5 nm) was done by XPS. The atomic percentages (%) of carbon, nitrogen,

oxygen, fluorine and copper are presented in Table 1. Results for pristine—i.e., non-functionalized—ND are shown for comparison, together with ND@NH_2.

Figures S1 and S2 of Supplementary Information show the XPS results for the samples ND@βNH-TPP*p*CF_3-Cu(II) and ND@βNH-TPP*p*CF_3, respectively. The C1s, N1s, O1s and F1s XPS spectra were similar for both samples.

Table 1. Surface atomic percentages of the elements for pristine ND, ND@NH_2, ND@βNH-TPP*p*CF_3-Cu(II) and ND@βNH-TPP*p*CF_3 obtained from XPS.

Sample	C 1s	N 1s	O 1s	F 1s	Cu 2p
Pristine NDs [1]	91.6	2.1	6.3	-	-
ND@NH_2 [1]	96.0	2.1	1.9	-	-
ND@βNH-TPP*p*CF_3-Cu(II)	94.7	2.0	1.4	1.8	0.06
ND@βNH-TPP$_p$$CF_3$	91.2	2.2	3.4	3.2	-

[1] Data from [40].

Detailed analysis of the XPS spectra is given in the SI. The results confirm the anchoring of the complexes.

From the compositional analysis shown in Table 1, a Cu percentage of 0.06 at.% in ND@βNH-TPP*p*CF_3-Cu(II) and a F percentage of 3.2 at.% at in ND@βNH-TPP*p*CF_3 were determined. These results indicate that amine groups from ND materials reacted with the nitro-porphyrin derivatives, displaying 0.050 mmol of metalloporphyrin **1** per gram of ND@βNH-TPP*p*CF_3-Cu(II) and 0.215 mmol of porphyrin **2** per gram of ND@βNH-TPP*p*CF_3.

In Figure 1, the normalized fluorescence emission spectra of ND@βNH-TPP*p*CF_3 (blue line), nitro-porphyrin **2** (black line) and ND@NH_2 (grey line) are displayed, with excitation at 420 nm using *N*,*N*-dimethylformamide (DMF) as solvent. The fluorescence spectrum of nitro-porphyrin **2**-immobilized nanodiamonds (ND@βNH-TPP*p*CF_3) is similar to that of the non-immobilized nitro-porphyrin **2** over the whole emission wavelength range (575 to 775 nm). In particular, two strong emission bands at 650 and 720 nm are present. Thus, qualitative analysis of the fluorescence emission spectrum of ND@βNH-TPP*p*CF_3 evidences that the energy of the excited state of porphyrin **2** is not changed by the presence of the material, probably due to the presence of a non-conjugated linker.

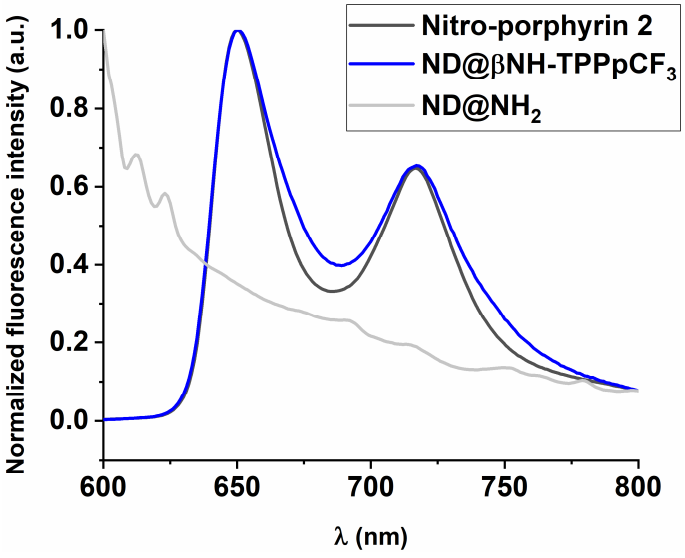

Figure 1. Normalized fluorescence emission spectra of ND@βNH-TPP*p*CF_3 (blue line), ND@NH_2 (grey line), and nitro-porphyrin **2** (black line) in DMF with excitation at 420 nm.

The normalized UV–Vis absorption spectra of ND@NH_2 (grey line), ND@βNH-TPP*p*CF_3 (blue line) and nitro-porphyrin **2** (black line) dispersed in *N*,*N*-dimethylformamide are presented in Figure 2. ND@βNH-TPP*p*CF_3 clearly shows the typical Soret band at 425 nm with a blue shift of 14 nm relatively to the nitro-porphyrin **2** free base. This blue shift is an unequivocal confirmation that the ipso-nitro substitution reaction occurred and an amine covalent linkage between the porphyrin and the NDs is present.

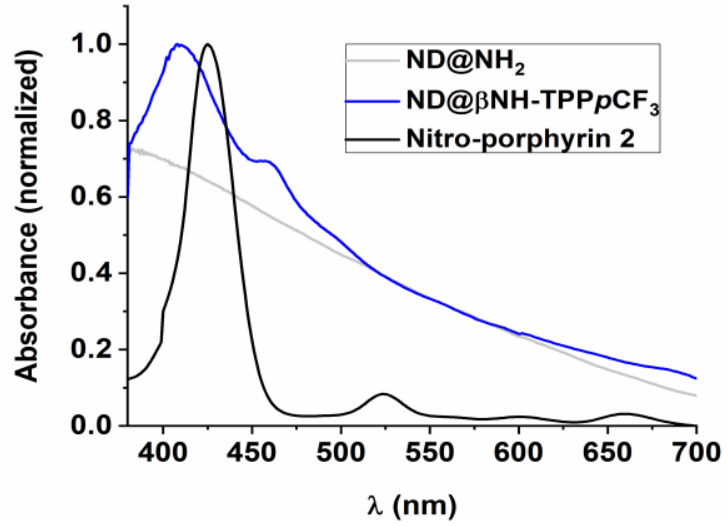

Figure 2. Normalized UV–Vis absorption spectra of ND@NH_2 (grey line), ND@βNH-TPP*p*CF_3 (blue line) and nitro-porphyrin **2** (black line) in DMF.

Figure 3 shows the infrared spectroscopic analysis of ND@βNH-TPP*p*CF_3-Cu(II) (red line) and ND@βNH-TPP*p*CF_3 (blue line), compared with the amine-functionalized nanodiamonds (ND@NH_2) (grey line). In the 2950–2850 and 1660–1630 cm^{-1} intervals, all IR spectra show signals characteristic for C–H stretching and amide C=O stretching vibrations, respectively. Moreover, between 1300 and 1700 cm^{-1}, both spectra of ND@βNH-TPP*p*CF_3-Cu(II) and ND@βNH-TPP*p*CF_3 present peaks at 1460 cm^{-1} (C–H bending) and 1350–1330 cm^{-1} (C–F stretching), validating the anchoring of the nitro-porphyrins (**1** and **2**) to the ND materials.

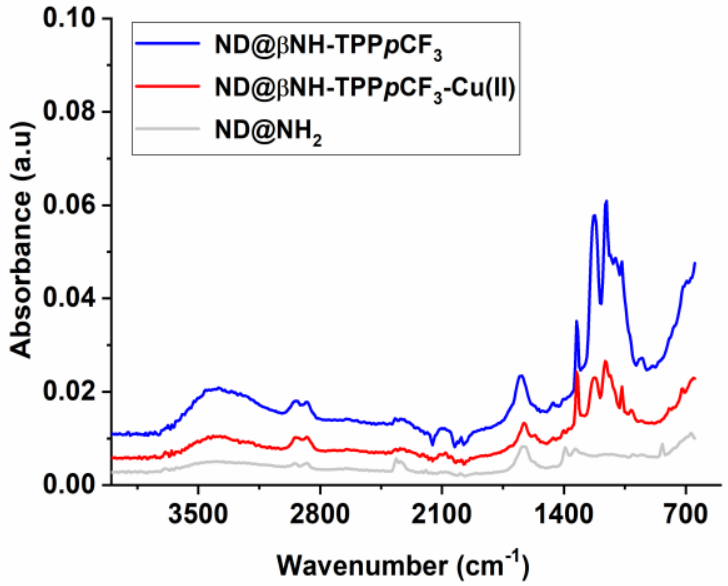

Figure 3. FT-IR spectra of ND@NH_2 (grey line), ND@βNH-TPP*p*CF_3-Cu(II) (red line) and ND@βNH-TPP*p*CF_3 (blue line).

Additionally, the quantification of the nitro-porphyrin (**1** and **2**) content for all three different functionalized NDs was performed using TG-DSC measurements between 30 and 800 °C (Figure S4a–c). By analysis and comparison with the TG-DSC curves of ND@NH_2, calculated weight losses of ND@βNH-TPP*p*CF_3-Cu(II) and ND@βNH-TPP*p*CF_3 were 5.6% and 6.3%, respectively, corresponding to 0.059 mmol/g ND of metalloporphyrin **1** and 0.071 mmol/g ND of porphyrin **2**.

2.2. Cytotoxic and Genotoxic Evaluation of Porphyrin-Functionalized Nanodiamonds in Allium Cepa Assay

Despite previous findings that NDs are non-cytotoxic for different types of cells and have higher biocompatibility when compared with all other nanocarbon-based materials (for instance, carbon nanotubes, fullerenes, graphene oxide, etc.) [36,48,49], recent studies showed that the cytotoxicity activity of NDs is correlated with their surface functionalities [50–52]. As an example, Marcon et al. demonstrated that ND functionalized with –COOH was highly toxic to Xenopus frog embryos, even at a low concentration (2 mg/L), in comparison to the embryotoxicity potential of ND with –OH or –NH_2 [50].

Our results, described in Supplementary Information, showed that the cytotoxicity and genotoxic potential of ND were not impacted by functionalizing them with the TPP*p*CF_3 porphyrin, and consequently, a non-phytotoxic porphyrin–nanodiamond hybrid nanomaterial was successfully prepared (Figure S5a–e).

2.3. Catalytic Oxidation Experiments

As stated above, cyclohexene oxidation products are of great interest in industry [33,34]. Therefore, to assess the application of copper-based ND@βNH-TPP*p*CF_3-Cu(II) as potential reusable catalysts, this new ND hybrid material was evaluated as catalyst in cyclohexene oxidation, using O_2 as a green oxidant (Scheme 3).

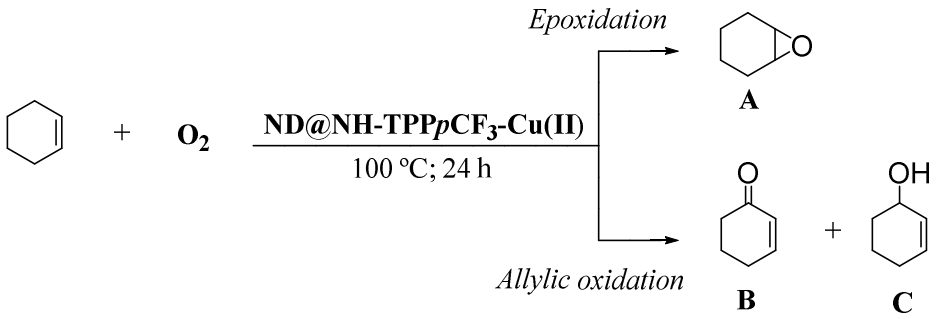

Scheme 3. Products of cyclohexene oxidation catalyzed by ND@βNH-TPP*p*CF_3-Cu(II). (A = 1,2-epoxycyclohexane; B = cyclohexen-1-one; C = 2-cyclohexen-1-ol).

Appropriate amounts of cyclohexene and ND@βNH-TPP*p*CF_3-Cu(II) catalyst were added in a reactor. After reaction at 100 °C, with O_2 (4 bar), for 24 h, cyclohexene conversion and product selectivity were determined by gas chromatography (GC) and gas chromatography-mass spectrometry (GC-MS), using aliquots from the reaction mixture. The results of conversion of cyclohexene and product selectivity are shown in Figure 4.

A cyclohexene conversion of 53% was obtained, with major products being 2-cyclohexen-1-one (B—39%) and 2-cyclohexen-1-ol (C—56%). This trend may be attributed to cyclohexene allylic products [53,54]. It is also worth mentioning the remarkable turnover number (TON) ≈ 265,000 achieved, using O_2 as green oxidant, in the total absence of sacrificial additives, whereas in the literature only TONs from 1210 to ≈200,000 were reported for the same oxidation reaction [55–57]. The ≈200,000 TON value refers to a previous publication of Pereira and co-workers, also using a copper metalloporphyrin but immobilized in magnetic nanoparticles [55]. A larger value was reported by other authors, but for the epoxidation reaction [58]. In this work, we obtained mainly the double bond products 2-cyclohexen-1-one and 2-cyclohexen-1-ol, as referred to above—that is, allylic oxidation products.

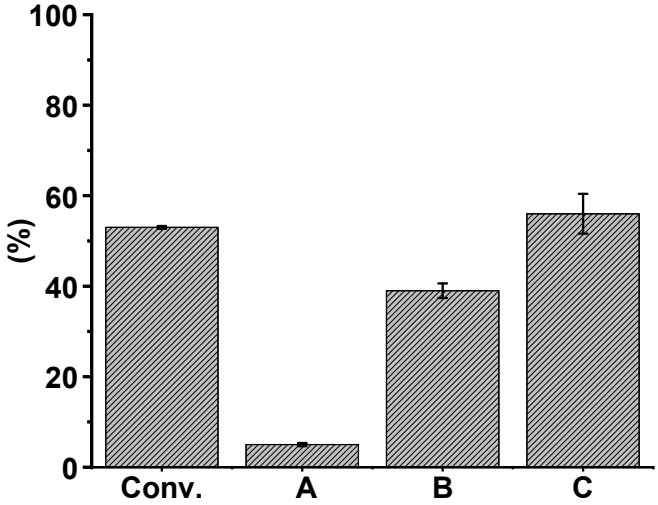

Figure 4. Conversion of cyclohexene (%) and product selectivity (%) (A = 1,2-epoxycyclohexane; B = cyclohexen-1-one; C = 2-cyclohexen-1-ol) when using ND@βNH-TPP*p*CF_3-Cu(II) as catalyst.

Additionally, nanodiamond-immobilized porphyrin (ND@βNH-TPP*p*CF_3-Cu(II)) could be separated from the reaction mixtures by centrifugation, and its recyclability was evaluated. The solid materials (ND@βNH-TPP*p*CF_3-Cu(II)) were washed three times with CH_2Cl_2 and three times with CH_3CN, then dried at 60 °C for 4 h and reused in the next catalytic cycle. The results are presented in Figure 5. The recycling experiments revealed good stability of the catalyst up to three cycles. Given the high catalyst dispersibility in cyclohexene, the observed slight decrease in the activity over the three cycles may be attributed to catalyst loss after decantation in each run.

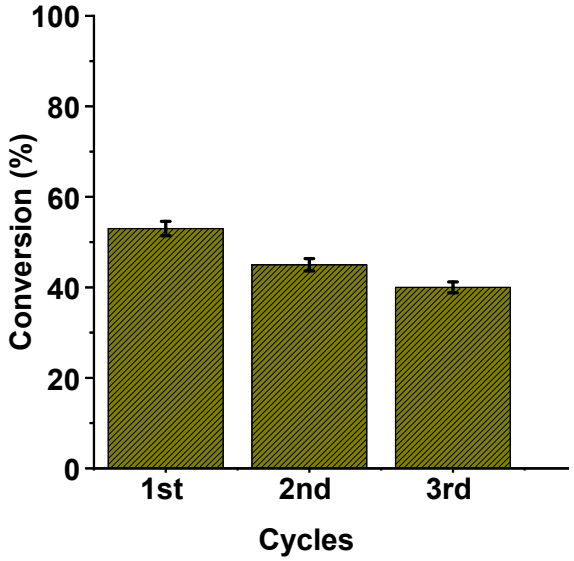

Figure 5. Recycling experiments of ND@βNH-TPP*p*CF_3-Cu(II) in the oxidation of cyclohexene. Data represent the mean ± standard error (n = 3).

3. Materials and Methods

3.1. Characterization of Chemicals and Materials

Reagents and solvents were purchased from Fluorochem (Derbyshire, UK) and/or Sigma-Aldrich (Lisbon, Portugal). All solvents and chemicals were purified and/or dried by methods from literature [59]. Amine functionalized nanodiamonds (ND@NH_2, UDiamond, Amine P) were purchased from Carbodeon, Finland. Nanodiamonds (NDs) with a primary average particle size of 5 nm

were obtained through detonation synthesis using a mixture of 2,4,6-trinitrotoluene (TNT) and 1,3,5-trinitroperhydro-1,3,5-triazine (RDX) high explosives as precursors. Boiling acid treatment was used to remove the amorphous carbon and impurities from the detonation soot to create the purified ND powder. Amine functionalization was subsequently done by heating the ND material for several hours in a gas atmosphere comprising ammonia gas.

XPS analyses were carried out in a Kratos AXIS Ultra HSA spectrometer (CEMUP, Porto, Portugal). All analysis was performed using the following conditions: monochromatic AlKα X-ray source (1486.7 eV), at 15 kV (90 W), in fixed analyzer transmission mode. Data acquisition was carried out using a pressure lower than 1×10^{-6} Pa. Survey and multi-region spectra were obtained at C 1s, O 1s, N 1s, F 1s and Cu 2p (this one only for the Cu containing sample) photoelectron peaks. The modelling of the spectra was performed using the CASA XPS program (Clearwater, FL, United States).

Fluorescence spectra were acquired on a Horiba-Jobin-Ivon Fluorolog 322 spectrofluorometer, using a quartz cuvette and *N*,*N*-dimethylformamide as solvent. All fluorescence emission spectra were normalized according to maximum intensity (from 0 to 1). FT-IR spectra were recorded on a Cary 630 FT-IR spectrometer using ≈20–25 mg of each sample, with Microlab PC software and ATR sampling unit with a resolution of 8 cm^{-1} and scan range of 4000 to 700 cm^{-1}. Gas chromatography (GC) analysis was carried out on a HP-Agilent 6890 chromatograph with Agilent GC software (Santa Clara, CA, United States), equipped with ionization detector (FID) (Santa Clara, CA, United States), and a HP-5 chromatographic column, non-polar (5% diphenyl, 95% dimethylpolysiloxane (30 m × 0.32 mm). GC-MS analysis was performed on a Hewlett-Packard 5973 MSD spectrometer (Santa Clara, CA, United States) (using EI = 70 eV), coupled to a Hewlett-Packard Agilent 6890 chromatograph (Santa Clara, CA, United States), and equipped with a HP-5 MS chromatographic column (30 m × 0.25 mm). The analyses were performed using the following chromatographic conditions: initial temperature 40 °C, rate 10 °C min^{-1}, final temperature 200 °C and gas flow of 1.41 $mL.min^{-1}$. Conversion and selectivity were calculated based on peak areas of GC. The identification and qualification of the peaks was confirmed by comparison of the mass spectra and retention times against *p*-xylene as external standard. Thermogravimetric analyses were performed on a Perkin-Elmer STA 6000 (Shelton, CT, United States) simultaneous TG-DSC instrument in a range between 25 °C and 800 °C.

3.2. Synthesis of Porphyrin Precursors and Metalloporphyrins

The synthesis of 2-nitro-5,10,15,20-tetra(4-trifluoromethylphenyl) porphyrinato copper(II) (**1**) and 2-nitro-5,10,15,20-tetra(4-trifluoromethylphenyl)porphyrin (**2**) was reported elsewhere [30]. Their synthesis was repeated at least three times and characterization data (^{1}H nuclear magnetic resonance (NMR) signals and mass spectra) are in agreement with the literature [30].

3.3. Immobilization of Nitro-Functionalized Porphyrins **1** *and* **2** *onto ND@NH$_2$*

ND@NH_2 (0.5 g) with the desired porphyrin **1** or porphyrin **2** (0.0825 mmol) and cesium carbonate (Cs_2CO_3) (0.165 mmol; 54 mg) in dry dimethoxyethane (DME) (50 mL) were stirred at 85 °C for 24 h. The resulting materials were filtered and washed three times with each of the following solvents—dimethoxyethane, dichloromethane, ethyl acetate and acetonitrile, to rinse away non-reacted porphyrin **1** or **2**. The obtained materials, ND@βNH-TPP*p*CF_3-Cu(II) and ND@βNH-TPP*p*CF_3, were then dried for 24 h.

3.4. Cytotoxic and Genotoxic Evaluation of Porphyrin-Functionalized Nanodiamonds in Allium Cepa Assays

Pesticide-free *A. cepa* seeds were purchased from Isla (Isla Sementes Ltd.a., Porto Alegre, RS, Brazil). The *A. cepa* assays were carried out according to literature [42,60]. The seeds were placed to germinate at 23 ± 2 °C under a photoperiod of 12 h light/12 h dark for 96 h. 30 seeds were continuously exposed to an aqueous solution (pure or containing NDs at 10, 50 and 100 $mg.L^{-1}$). All tests were performed in triplicate, totaling 90 seeds per group. The germination index (GI) was calculated after 96 h.

The root length index (RLI) was measured using a digital caliper (Digimess, São Paulo, SP, Brazil) after 96 h of the germination. Then, the roots were collected and prepared for the mitotic index (MI), nuclear abnormality index (NAI) and micronucleus index (MNI) determination. After the collection, the roots were fixed in Carnoy Solution 3:1 (alcohol/acetic acid) during 8 h and then stored at 4 °C. After that, the fixed roots were washed with tap water and hydrolyzed in 1 N HCl at 60 °C for 10 min. Next, they were washed again and stained with Schiff's reagent for 2 h. Subsequently, the root meristems were slightly smashed in a drop of 45% acetic carmine. Finally, 5 slides were prepared per group and imaged using an optical microscope (Nikon, Tokyo, Japan) at a 400× magnification. 1000 cells were evaluated per slide, resulting in 5000 cells checked per treatment. All experiments were performed in triplicate and the GI, REI, MI, NAI, and MNI values were submitted to Paired Sample t Test ($p \leq 0.05$) for comparison of pairs of means.

3.5. Procedure for Oxidation of Cyclohexene Using ND@βNH-TPPpCF$_3$-Cu(II) as Catalyst

ND@βNH-TPP*p*CF_3-Cu(II) (4 mg; 19.8×10^{-8} mol of Cu) as catalyst and cyclohexene (10 mL; 0.099 mol) as substrate were added to a reactor and then charged with oxygen (O_2, 4 atm). The reaction mixture was maintained at 100 °C, during 24 h, under stirring. After this time, the reactor was depressurized and an aliquot from the crude reaction was analyzed by GC.

In the reutilization tests, after each catalytic cycle, the copper(II) porphyrin-functionalized nanodiamonds (ND@βNH-TPP*p*CF_3-Cu(II)) were separated from the reaction mixture by centrifugation and the supernatant solution by decantation. Then, the nanomaterials (ND@βNH-TPP*p*CF_3-Cu(II)) were washed using acetonitrile (three times, using 4 mL) and dichloromethane (three times, using 4 mL), dried at 60 °C, during 4 h, and used in the next catalytic cycle. No catalyst adjustment was made after each run.

4. Conclusions

We demonstrated that the β-*ipso*-nitro-aromatic nucleophilic substitution of amine-functionalized NDs with β-nitro substituted porphyrins is an innovative and efficient approach to prepare covalently linked hybrid porphyrin–nanodiamond materials. The nanocomposites' characterization by XPS, fluorescence, UV–Vis spectroscopy, IR spectroscopy and TGA-DSC unequivocally corroborated the effective grafting of the nitro-porphyrins (**1** and **2**) onto the amine-functionalized NDs. Moreover, our study revealed the hybrid nanodiamond–copper(II)–porphyrin as the best ever reported allylic cyclohexene oxidation catalyst (TON ≈ 265,000), using only O_2 as a "green" oxidant, in the absence of reductants/solvents. Furthermore, the material could be recovered by centrifugation and used again in three consecutive catalytic cycles without major loss of activity. Moreover, this porphyrin–nanodiamond catalyst, under similar reaction conditions, may be able to oxidize other substrates, namely, α-pinene, β-pinene and thiophenol derivatives. In addition, no ecotoxic and genotoxic effects were observed for ND@NH_2 and ND@βNH-TPP*p*CF_3 materials, using *Allium cepa* as the plant model.

The findings described herein allow us to foresee the significance of materials of this type in oxidative catalysis, and their potential in biomedical applications.

Supplementary Materials: The following are available online at http://www.mdpi.com/2073-4344/10/12/1402/s1. Figure S1: XPS results of hybrid sample ND@βNH-TPP*p*CF_3-Cu(II): C1s (a,b), N1s (c), O1s (d), F1s (e), Cu 2p (f). Figure S2: XPS results of hybrid sample ND@βNH-TPP*p*CF_3: C1s (a,b), N1s (c), O1s (d), F1s (e). Figure S3: Survey XPS spectra of ND@βNH-TPP*p*CF_3-Cu(II) (a) and ND@βNH-TPP*p*CF_3 (b). Figure S4: TG-DSC curves of: (a) ND@NH_2; (b) ND@βNH-TPP*p*CF_3-Cu(II); (c) ND@βNH-TPP*p*CF_3; weight loss (solid line); heat flow (dashed line). Figure S5: Effects of the ND@NH_2, ND@βNH-TPP*p*CF_3 and H_2O (control group) on (a) the germination index (GI); (b) the root elongation index (REI); (c) the mitotic index (MI); (d) the micronucleus index (MNI); and (e) the nuclear abnormality index (NAI) of the *A. cepa* cells. Data represent the mean ± standard error and different letters means significant difference among the groups ($p < 0.05$). *Allium cepa* seeds were exposed to three concentrations (10, 50 and 100 mg/L).

Author Contributions: Conceptualization, L.D.D.; S.A.C.C. and M.M.P.; methodology, L.D.D.; S.A.C.C. and M.M.P.; investigation, L.D.D., F.M.S.R. and M.D.S.; writing—original draft preparation, L.D.D., F.M.S.R., M.J.F.C., S.A.C.C., M.D.S., A.R.L.C., J.G.B., J.L.F., V.S.B. and M.M.P.; writing—review and editing, L.D.D., F.M.S.R., M.J.F.C., S.A.C.C.,

M.D.S., A.R.L.C., J.G.B., J.L.F., V.S.B. and M.M.P.; funding acquisition, S.A.C.C., J.G.B., J.L.F., V.S.B. and M.M.P. All authors have read and agreed to the published version of the manuscript.

Funding: This research was funded by FCT—Foundation for Science and Technology, I.P., under projects UIDB/00313/2020; PTDC/QUI-OUT/27996/2017 (DUALPI); POCI-01-0145-FEDER-027996; POCI-01–0145-FEDER- 016387; UIDB/50006/2020 (Associate Laboratory for Green Chemistry—LAQV); MATIS (CENTRO-010145-FEDER-00014); Base Funding—UIDB/50020/2020 of the Associate Laboratory LSRE-LCM—funded by national funds through FCT/MCTES (PIDDAC); and 5625-DRI-DAAD-2020/21. SACC also acknowledges FCT Investigador FCT program (IF/01381/2013/CP1160/CT0007) and Scientific Employment Stimulus - Institutional Call (CEECINST/00102/2018). The authors also thank Fundação de Amparo à Pesquisa do Estado de São Paulo (FAPESP) for CEPOF 2013/07276-1, and INCT "Basic Optics and Applied to Life Sciences" (FAPESP 2014/50857-8, CNPq 465360/2014-9). A.R.L. Caires acknowledges CAPES-PrInt funding program (grant number 88887.353061/2019-00 and 88881.311921/2018-01). J.G.B. thanks the Dutch Research Council (NWO) for funding as a part of the Open Technology Programme (project number 16361). L.D. Dias thanks FAPESP for the Post-doc grant 2019/13569-8. F.M.S.R. thanks FCT for the PhD grant (PD/BD/114340/2016).

Acknowledgments: The authors acknowledge Carlos Sá (CEMUP) for the assistance with XPS analyses.

Conflicts of Interest: The authors declare no conflict of interest.

References

1. Danilenko, V.V. On the history of the discovery of nanodiamond synthesis. *Phys. Solid State* **2004**, *46*, 595–599. [CrossRef]
2. Mochalin, V.N.; Shenderova, O.; Ho, D.; Gogotsi, Y. The properties and applications of nanodiamonds. *Nat. Nanotechnol.* **2012**, *7*, 11–23. [CrossRef]
3. Lin, Y.; Sun, X.; Su, D.S.; Centi, G.; Perathoner, S. Catalysis by hybrid sp2/sp3nanodiamonds and their role in the design of advanced nanocarbon materials. *Chem. Soc. Rev.* **2018**, *47*, 8438–8473. [CrossRef]
4. Lai, H.; Chen, F.; Lu, M.; Stenzel, M.H.; Xiao, P. Polypeptide-Grafted Nanodiamonds for Controlled Release of Melittin to Treat Breast Cancer. *ACS Macro Lett.* **2017**, *6*, 796–801. [CrossRef]
5. Ishchenko, A.A.; Mchedlov-Petrossyan, N.O.; Kriklya, N.N.; Kryshtal, A.P.; Ōsawa, E.; Kulinich, A.V. Interaction of Polymethine Dyes with Detonation Nanodiamonds. *ChemPhysChem* **2019**, *20*, 1028–1035. [CrossRef]
6. Sinolits, A.V.; Chernysheva, M.G.; Matveeva, O.D.; Popov, A.G.; Badun, G.A. Chitosan adsorption on nanodiamonds: Stability and mechanism. *Fuller Nanotub. Carbon Nanostruct.* **2019**, *28*, 299–303. [CrossRef]
7. Guo, H.; Hu, H.; Yu, X.; Naito, K.; Zhang, Q. Covalent Functionalization of Nanodiamonds with Natural Amino Acids and Ascorbic Acids. *J. Nanosci. Nanotechnol.* **2019**, *19*, 7574–7583. [CrossRef]
8. Patoary, N.H.; Rai, A.; Patel, K.P.; Rebecca, A.; Zhang, W.; Ulrich, A.J.; Galib, M.; Desai, T.; Zivanovic, S.; Yousufuddin, M.; et al. Directed covalent assembly of nanodiamonds into thin films. *Diam. Relat. Mater.* **2020**, *101*, 9. [CrossRef]
9. Pastrana-Martínez, L.M.; Morales-Torres, S.; Carabineiro, S.A.C.; Buijnsters, J.G.; Faria, J.L.; Figueiredo, J.L.; Silva, A.M. Nanodiamond-TiO2Composites for Heterogeneous Photocatalysis. *ChemPlusChem* **2013**, *78*, 750. [CrossRef]
10. Nunes-Pereira, J.; Silva, A.R.; Ribeiro, C.; Carabineiro, S.A.C.; Buijnsters, J.G.; Lanceros-Méndez, S. Nanodiamonds/poly(vinylidene fluoride) composites for tissue engineering applications. *Compos. Part B Eng.* **2017**, *111*, 37–44. [CrossRef]
11. Whitlow, J.; Pacelli, S.; Paul, A. Multifunctional nanodiamonds in regenerative medicine: Recent advances and future directions. *J. Control. Release* **2017**, *261*, 62–86. [CrossRef]
12. Day, A.H.; Adams, S.J.; Gines, L.; Williams, O.A.; Johnson, B.R.; Fallis, I.A.; Loveridge, E.J.; Bahra, G.S.; Oyston, P.C.; Herrera, J.M.; et al. Synthetic routes, characterization and photophysical properties of luminescent, surface functionalized nanodiamonds. *Carbon* **2019**, *152*, 335–343. [CrossRef]
13. Solarska-Ściuk, K.; Kleszczyńska, H. Possibilities of nanodiamonds application—Biological and medical aspects. *Acta Pol. Pharm. Drug Res.* **2019**, *76*, 779–796. [CrossRef]
14. Kumar, S.; Nehra, M.; Kedia, D.; Dilbaghi, N.; Tankeshwar, K.; Kim, K.-H. Nanodiamonds: Emerging face of future nanotechnology. *Carbon* **2019**, *143*, 678–699. [CrossRef]
15. Sangiao, E.T.; Holban, A.M.; Gestal, M.C. Applications of Nanodiamonds in the Detection and Therapy of Infectious Diseases. *Materials* **2019**, *12*, 1639. [CrossRef]

16. Matshitse, R.; Ngoy, B.P.; Managa, M.; Mack, J.; Nyokong, T. Photophysical properties and photodynamic therapy activities of detonated nanodiamonds-BODIPY-phthalocyanines nanoassemblies. *Photodiagnosis Photodyn. Ther.* **2019**, *26*, 101–110. [CrossRef]
17. Matshitse, R.; Managa, M.; Nyokong, T. The modulation of the photophysical and photodynamic therapy activities of a phthalocyanine by detonation nanodiamonds: Comparison with graphene quantum dots and carbon nanodots. *Diam. Relat. Mater.* **2020**, *101*, 107617. [CrossRef]
18. Lai, H.; Stenzel, M.H.; Xiao, P. Surface engineering and applications of nanodiamonds in cancer treatment and imaging. *Int. Mater. Rev.* **2020**, *65*, 189–225. [CrossRef]
19. Muller, O.; Pichot, V.; Merlat, L.; Schmidlin, L.; Spitzer, D. Nonlinear optical behavior of porphyrin functionalized nanodiamonds: An efficient material for optical power limiting. *Appl. Opt.* **2016**, *55*, 3801–3808. [CrossRef]
20. Muller, O.; Pichot, V.; Merlat, L.; Spitzer, D. Optical limiting properties of surface functionalized nanodiamonds probed by the Z-scan method. *Sci. Rep.* **2019**, *9*, 1–11. [CrossRef]
21. Afandi, A.; Howkins, A.; Boyd, I.W.; Jackman, R.B. Nanodiamonds for device applications: An investigation of the properties of boron-doped detonation nanodiamonds. *Sci. Rep.* **2018**, *8*, 1–10. [CrossRef] [PubMed]
22. Radulaski, M.; Zhang, J.L.; Tzeng, Y.; Lagoudakis, K.G.; Ishiwata, H.; Dory, C.; Fischer, K.A.; Kelaita, Y.A.; Sun, S.; Maurer, P.C.; et al. Nanodiamond Integration with Photonic Devices. *Laser Photon Rev.* **2019**, *13*, 14. [CrossRef]
23. Shenderova, O.; Vargas, A.; Turner, S.; Ivanov, D.M.; Ivanov, M.G. Nanodiamond-Based Nanolubricants: Investigation of Friction Surfaces. *Tribol. Trans.* **2014**, *57*, 1051–1057. [CrossRef]
24. Marko, M.; Kyle, J.P.; Branson, B.; Terrell, E.J. Tribological Improvements of Dispersed Nanodiamond Additives in Lubricating Mineral Oil. *J. Tribol. Trans. ASME* **2015**, *137*, 7. [CrossRef]
25. Picollo, F.; Mino, L.; Battiato, A.; Tchernij, S.D.; Forneris, J.; Martina, K.; Sacco, M.; Tagliapietra, S.; Vittone, E.; Olivero, P.; et al. Synthesis and characterization of porphyrin functionalized nanodiamonds. *Diam. Relat. Mater.* **2019**, *91*, 22–28. [CrossRef]
26. Arnaut, L.G.; Pereira, M.M.; Dąbrowski, J.M.; Silva, E.F.F.; Schaberle, F.A.; Abreu, A.R.; Rocha, L.B.; Barsan, M.M.; Urbańska, K.; Stochel, G.; et al. Photodynamic Therapy Efficacy Enhanced by Dynamics: The Role of Charge Transfer and Photostability in the Selection of Photosensitizers. *Chem. A Eur. J.* **2014**, *20*, 5346–5357. [CrossRef]
27. Gonçalves, N.P.F.; Simões, A.V.C.; Abreu, A.R.; Abrunhosa, A.J.; Dąbrowski, J.M.; Pereira, M.M. Synthesis and biological distribution study of a new carbon-11 labeled porphyrin for PET imaging. Photochemical and biological characterization of the non-labeled porphyrin. *J. Porphyr. Phthalocyanines* **2015**, *19*, 946–955. [CrossRef]
28. Simões, A.V.C.; Pinto, S.M.A.; Calvete, M.J.F.; Gomes, C.M.F.; Ferreira, N.C.; Castelo-Branco, M.; Llop, J.; Pereira, M.M.; Abrunhosa, A.J. Synthesis of a new 18F labeled porphyrin for potential application in positron emission tomography. In vivo imaging and cellular uptake. *RSC Adv.* **2015**, *5*, 99540–99546. [CrossRef]
29. Pucelik, B.; Paczyński, R.; Dubin, G.; Pereira, M.M.; Arnaut, L.G.; Dąbrowski, J.M. Properties of halogenated and sulfonated porphyrins relevant for the selection of photosensitizers in anticancer and antimicrobial therapies. *PLoS ONE* **2017**, *12*, e0185984. [CrossRef]
30. Dias, L.D.; Carrilho, R.M.B.; Henriques, C.A.; Calvete, M.J.F.; Masdeu-Bultó, A.M.; Claver, C.; Rossi, L.M.; Pereira, M.M. Hybrid Metalloporphyrin Magnetic Nanoparticles as Catalysts for Sequential Transformation of Alkenes and CO2 into Cyclic Carbonates. *ChemCatChem* **2018**, *10*, 2792–2803. [CrossRef]
31. Dias, L.D.; De Carvalho, A.L.M.B.; Pinto, S.M.A.; Aquino, G.L.B.; Calvete, M.J.F.; Rossi, L.M.; Marques, M.P.M.; Pereira, M.M. Bioinspired-Metalloporphyrin Magnetic Nanocomposite as a Reusable Catalyst for Synthesis of Diastereomeric (−)-Isopulegol Epoxide: Anticancer Activity Against Human Osteosarcoma Cells (MG-63). *Molecules* **2019**, *24*, 52. [CrossRef] [PubMed]
32. Chevallier, E.; Scorsone, E.; Girard, H.; Pichot, V.; Spitzer, D.; Bergonzo, P. Metalloporphyrin-functionalised diamond nano-particles as sensitive layer for nitroaromatic vapours detection at room-temperature. *Sens. Actuators B Chem.* **2010**, *151*, 191–197. [CrossRef]
33. Sato, K.; Aoki, M.; Noyori, R. A "Green" Route to Adipic Acid: Direct Oxidation of Cyclohexenes with 30 Percent Hydrogen Peroxide. *Science* **1998**, *281*, 1646–1647. [CrossRef] [PubMed]
34. Nowak, I.; Ziolek, M. Effect of texture and structure on the catalytic activity of mesoporous niobosilicates for the oxidation of cyclohexene. *Microporous Mesoporous Mater.* **2005**, *78*, 281–288. [CrossRef]

35. Cao, H.; Zhu, B.; Yang, Y.; Xu, L.; Yu, L.; Xu, Q. Recent advances on controllable and selective catalytic oxidation of cyclohexene. *Chin. J. Catal.* **2018**, *39*, 899–907. [CrossRef]
36. Xing, Y.; Dai, L. Nanodiamonds for nanomedicine. *Nanomedicine* **2009**, *4*, 207–218. [CrossRef]
37. Rocha, R.P.; Sousa, J.P.; Silva, A.M.; Pereira, M.F.; Figueiredo, J. Catalytic activity and stability of multiwalled carbon nanotubes in catalytic wet air oxidation of oxalic acid: The role of the basic nature induced by the surface chemistry. *Appl. Catal. B Environ.* **2011**, *104*, 330–336. [CrossRef]
38. Sundar, L.S.; Anjum, N.A.; Ferro, M.; Pereira, E.; Singh, M.K.; Sousa, A.C.M. Biocompatibility and biotoxicity of in-situ synthesized carboxylated nanodiamond-cobalt oxide nanocomposite. *J. Mater. Sci. Technol.* **2017**, *33*, 879–888. [CrossRef]
39. Chernysheva, M.G.; Myasnikov, I.Y.; Badun, G.A.; Matorin, D.N.; Gabbasova, D.T.; Konstantinov, A.I.; Korobkov, V.I.; Kulikova, N.A. Humic substances alter the uptake and toxicity of nanodiamonds in wheat seedlings. *J. Soils Sediments* **2016**, *18*, 1335–1346. [CrossRef]
40. Pastrana-Martínez, L.M.; Figueiredo, J.L.; Carabineiro, S.A.; Buijnsters, J.G.; Figueiredo, J.L.; Silva, A.M.; Faria, J.L. Photocatalytic activity of functionalized nanodiamond-TiO2 composites towards water pollutants degradation under UV/Vis irradiation. *Appl. Surf. Sci.* **2018**, *458*, 839–848. [CrossRef]
41. Basiuk, V.A.; Terrazas, T.; Luna-Martínez, N.; Basiuk, E.V. Phytotoxicity of carbon nanotubes and nanodiamond in long-term assays with Cactaceae plant seedlings. *Fuller. Nanotub. Carbon Nanostruct.* **2018**, *27*, 141–149. [CrossRef]
42. Leme, D.M.; Marin-Morales, M.A. Allium cepa test in environmental monitoring: A review on its application. *Mutat. Res. Rev. Mutat. Res.* **2009**, *682*, 71–81. [CrossRef] [PubMed]
43. Gonsalves, A.M.D.R.; Varejão, J.M.T.B.; Pereira, M.M. Some new aspects related to the synthesis ofmeso-substituted porphyrins. *J. Heterocycl. Chem.* **1991**, *28*, 635–640. [CrossRef]
44. Crossley, M.J.; King, L.G.; Pyke, S.M. A new and highly efficient synthesis of hydroxyporphyrins. *Tetrahedron* **1987**, *43*, 4569–4577. [CrossRef]
45. Crossley, M.J.; King, L.G.; Pyke, S.M.; Tansey, C.W. Reaction of 5-nitro-octaethylporphyrins with nucleophiles. *J. Porphyr. Phthalocyanines* **2002**, *6*, 685–694. [CrossRef]
46. Rebelo, S.L.H.; Gonçalves, A.R.; Pereira, M.M.; Simões, M.M.; Neves, M.G.P.M.S.; Cavaleiro, J.A.S. Epoxidation reactions with hydrogen peroxide activated by a novel heterogeneous metalloporphyrin catalyst. *J. Mol. Catal. A Chem.* **2006**, *256*, 321–323. [CrossRef]
47. Vicente, M.G.H.; Smith, K.M. Syntheses and Functionalizations of Porphyrin Macrocycles. *Curr. Org. Synth.* **2014**, *11*, 3–28. [CrossRef]
48. Zhang, X.; Hu, W.; Li, J.; Tao, L.; Wei, Y. A comparative study of cellular uptake and cytotoxicity of multi-walled carbon nanotubes, graphene oxide, and nanodiamond. *Toxicol. Res.* **2012**, *1*, 62–68. [CrossRef]
49. Maas, M. Carbon Nanomaterials as Antibacterial Colloids. *Materials* **2016**, *9*, 617. [CrossRef]
50. Marcon, L.; Riquet, F.; Vicogne, D.; Szunerits, S.; Bodart, J.-F.; Boukherroub, R. Cellular and in vivo toxicity of functionalized nanodiamond in Xenopus embryos. *J. Mater. Chem.* **2010**, *20*, 8064–8069. [CrossRef]
51. Zhang, Y.; Zhang, W.; Fedutik, Y.; Mao, Z.; Gao, C. Nanodiamonds of Different Surface Chemistry Influence the Toxicity and Differentiation of Rat Bone Mesenchymal Stem Cells In Vitro. *J. Nanosci. Nanotechnol.* **2019**, *19*, 5426–5434. [CrossRef]
52. Fusco, L.; Avitabile, E.; Armuzza, V.; Orecchioni, M.; Istif, A.; Bedognetti, D.; Da Ros, T.; Delogu, L.G. Impact of the surface functionalization on nanodiamond biocompatibility: A comprehensive view on human blood immune cells. *Carbon* **2020**, *160*, 390–404. [CrossRef]
53. Cohen, S.; Kozuch, S.; Hazan, C.; Shaik, S. Does Substrate Oxidation Determine the Regioselectivity of Cyclohexene and Propene Oxidation by Cytochrome P450? *J. Am. Chem. Soc.* **2006**, *128*, 11028–11029. [CrossRef]
54. Bohström, Z.; Rico-Lattes, I.; Holmberg, K. Oxidation of cyclohexene into adipic acid in aqueous dispersions of mesoporous oxides with built-in catalytical sites. *Green Chem.* **2010**, *12*, 1861–1869. [CrossRef]
55. Henriques, C.A.; Fernandes, A.; Rossi, L.M.; Ribeiro, M.F.; Calvete, M.J.F.; Pereira, M.M. Biologically Inspired and Magnetically Recoverable Copper Porphyrinic Catalysts: A Greener Approach for Oxidation of Hydrocarbons with Molecular Oxygen. *Adv. Funct. Mater.* **2016**, *26*, 3359–3368. [CrossRef]
56. Denekamp, I.M.; Antens, M.; Slot, T.K.; Rothenberg, G. Selective Catalytic Oxidation of Cyclohexene with Molecular Oxygen: Radical Versus Nonradical Pathways. *ChemCatChem* **2018**, *10*, 1035–1041. [CrossRef]

57. Li, C.; Zhao, Y.; Zhu, T.; Li, Y.; Ruan, J.; Li, G. Effective solvent-free oxidation of cyclohexene to allylic products with oxygen by mesoporous etched halloysite nanotube supported Co^{2+}. *RSC Adv.* **2018**, *8*, 14870–14878. [CrossRef]
58. Yang, G.; Du, H.; Liu, J.; Zhou, Z.; Hu, X.; Zhang, Z. Oxidation of olefins using molecular oxygen catalyzed by a part per million level of recyclable copper catalyst under mild conditions. *Green Chem.* **2017**, *19*, 675–681. [CrossRef]
59. Hill, A.G.; Angell, F.G.; Macdonald, A.M.G. Book reviews. *Analyst* **1967**, *92*, 537–538. [CrossRef]
60. Scherer, M.D.; Sposito, J.C.; Falco, W.F.; Grisolia, A.B.; Andrade, L.H.; Lima, S.; Machado, G.; Nascimento, V.A.; Gonçalves, D.A.; Wender, H.; et al. Cytotoxic and genotoxic effects of silver nanoparticles on meristematic cells of Allium cepa roots: A close analysis of particle size dependence. *Sci. Total. Environ.* **2019**, *660*, 459–467. [CrossRef]

Publisher's Note: MDPI stays neutral with regard to jurisdictional claims in published maps and institutional affiliations.

© 2020 by the authors. Licensee MDPI, Basel, Switzerland. This article is an open access article distributed under the terms and conditions of the Creative Commons Attribution (CC BY) license (http://creativecommons.org/licenses/by/4.0/).